Quantised transistor response to ion channels revealed by nonstationary noise analysis

2011 EPL 96 38005

(http://iopscience.iop.org/0295-5075/96/3/38005)

A Letters Journal Exploring the Frontiers of Physics

November 2011

EPL, **96** (2011) 38005
doi: 10.1209/0295-5075/96/38005

www.epljournal.org

Quantised transistor response to ion channels revealed by nonstationary noise analysis

C. Becker-Freyseng and P. Fromherz[a]

Department of Membrane and Neurophysics, Max Planck Institute for Biochemistry - Am Klopferspitz 18, D-82152 Martinsried/München, Germany, EU

received 4 July 2011; accepted in final form 12 September 2011
published online 19 October 2011

PACS 87.85.dh – Cells on a chip
PACS 73.50.Td – Noise processes and phenomena
PACS 87.16.Vy – Ion channels

Abstract – We report on the quantised response of a field-effect transistor to molecular ion channels in a biomembrane. HEK293-type cells overexpressing the Shaker B potassium channel were cultured on a silicon chip. An enhanced noise of the transistor is observed when the ion channels are activated. The analysis of the fluctuations in terms of binomial statistics identifies voltage quanta of about 1 μV on the gate. They are attributed to the channel currents that affect the gate voltage according to the Green's function of the cell-chip junction.

Introduction. – Biomembranes on a solid support have been considered in connection with biophysical processes such as mechanical fluctuations [1], protein diffusion [2], pattern formation [3], cell adhesion [4], cell motion [5], synaptic transmission [6], and neuroelectronic interfacing [7]. The electrical features of a supported membrane are determined by the current of ion channels, which gives rise to a voltage in the narrow space between the membrane and the support (fig. 1(a)). Considering the stochastic opening and closing of molecular ion channels [8–10], it is expected that the arising voltage fluctuations may be relevant for ionic processes in the membrane and electronic processes in the support. The transduction of an ionic membrane current into the electronic current in a transistor has been originally studied for neuronal excitation [11,12], and later for recombinant ion channels in cultured cells [13–15]. Those experiments referred to the average transistor signal. Voltage fluctuations have been observed in the absence of open channels and were assigned to the thermal noise of the cell-solid junction [16]. It is the goal of the present study to take advantage of the stochastic opening and closing of ion channels and of transistor recording in the electrical characterization of supported biomembranes and of bioelectronic interfacing.

The experiments were performed with the voltage-gated Shaker B potassium channel that had been overexpressed in HEK293-type cells [17–19]. Upon an intracellular stimulation by a patch-pipette, the changing membrane current was measured through the pipette and the changing extracellular voltage in the area of cell adhesion was probed with a transistor. The macroscopic recordings fluctuated around the nonstationary average signals due to the stochastic nature of the ion channels. For the current as well as for the voltage, we performed a nonstationary noise analysis [10,20–22], which compares the changing variance of an ensemble of signals with the changing average of the ensemble. At first, we address the theoretical background and describe the experimental issues. Then we present the recordings of pipette current and transistor voltage, estimate the magnitude of the voltage quanta and interpret them in terms of the current quanta and the features of the cell-solid junction.

Ion channels and core-coat conductor. – When a positive voltage step is applied to the cell, the probability p of the channels to be open is enhanced. For N_{ch} channel molecules, the variance of the number N of open channels is determined by binomial statistics [10] with

$$\sigma_{\mathrm{N}}^2 = (1-p)pN_{\mathrm{ch}}. \tag{1}$$

A parabolic relation is obtained between the variance and the expectation value of the membrane current according to eq. (2) for a well-defined current quantum i_{ch} [10] with a total membrane current $I_{\mathrm{M}} = i_{\mathrm{ch}}N$ and an expectation

[a]E-mail: fromherz@biochem.mpg.de

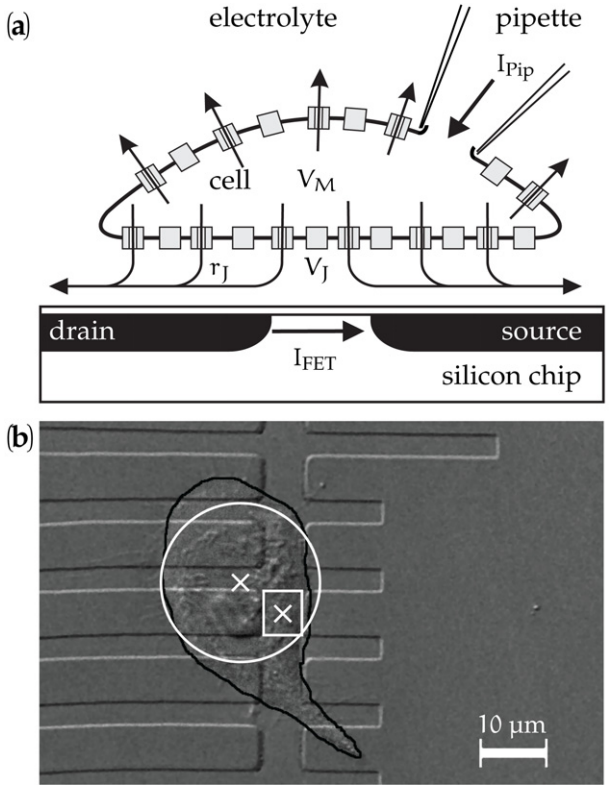

Fig. 1: Cell-transistor junction. (a) Schematic cross-section. The cell membrane with open and closed ion channels is joined to a micropipette. Not to scale: cell diameter around 20 μm, cell-chip distance around 50 nm, size of ion channel around 7 nm. An intracellular voltage V_M is applied through the pipette; it controls the open probability of the ion channels. The membrane current through the open channels (arrows) flows through the pipette (I_{Pip}). The current of the adherent membrane flows along an electrolyte film (sheet resistance r_J) between cell and support; it induces an extracellular voltage V_J on the open gate of the transistor. The modulation of the drain current I_{FET} is calibrated in terms of the extracellular voltage. (b) Micrograph of a HEK293-type cell on transistors with drains (left) and a common source (right). The gate of the recording transistor is marked by a frame. The area of adhesion (black line) is matched by a circle with a radius 12 μm. The crosses mark the centres of the circle and of the gate.

value $\langle I_M\rangle = i_{ch} p N_{ch}$,

$$\sigma^2_{IM} = i_{ch}\langle I_M\rangle - N_{ch}^{-1}\langle I_M\rangle^2. \tag{2}$$

With a supported cell, a portion of the current in the membrane with an area A_M flows through the adherent area $A_{JM} = \alpha_J A_M$ ($\alpha_J \leqslant 1$) and along an electrolyte film with a sheet resistance r_J (fig. 1(a)). It gives rise to a 2D profile of the extracellular voltage $V_J(\boldsymbol{x})$ in the cell-solid junction with the properties of a core-coat conductor [11]. The dynamics of the ion channels is far slower (in the range of a few milliseconds) than the time constant of the core-coat conductor (a few microseconds). The voltage profile is governed by the Poisson's equation $\nabla^2 V_J(\boldsymbol{x}) = -r_J i_{JM}(\boldsymbol{x})$ with a current per unit area $i_{JM}(\boldsymbol{x})$. With a Green's function $G_J(\boldsymbol{x},\boldsymbol{x}')$ defined by $\nabla^2 G_J(\boldsymbol{x},\boldsymbol{x}') = -\delta(\boldsymbol{x}-\boldsymbol{x}')$ and Dirichlet boundary conditions, we obtain

$$V_J(\boldsymbol{x}) = r_J \int_{A_{JM}} \mathrm{d}\boldsymbol{x}' G_J(\boldsymbol{x},\boldsymbol{x}') i_{JM}(\boldsymbol{x}'). \tag{3}$$

We assume that the cell membrane is homogeneous, the current fluctuations in different area elements are statistically independent, and the number of channel molecules in the attached membrane is constant for the short duration of a measurement. The expectation value and the variance of $i_{JM}(\boldsymbol{x}')$ are $\langle I_M\rangle/A_M$ and σ^2_{IM}/A_M, respectively. The profiles of the expectation value and the variance of $V_J(\boldsymbol{x})$ are given by eqs. (4) and (5) with spatial averages $\overline{G_J}(\boldsymbol{x})$ and $\overline{G_J^2}(\boldsymbol{x})$:

$$\begin{aligned}\langle V_J(\boldsymbol{x})\rangle &= r_J\langle I_M\rangle A_M^{-1}\int_{A_{JM}} \mathrm{d}\boldsymbol{x}' G_J(\boldsymbol{x},\boldsymbol{x}')\\ &= \alpha_J r_J \overline{G_J}(\boldsymbol{x})\langle I_M\rangle\end{aligned} \tag{4}$$

$$\begin{aligned}\sigma^2_{VJ}(\boldsymbol{x}) &= r_J^2\sigma^2_{IM}A_M^{-1}\int_{A_{JM}} \mathrm{d}\boldsymbol{x}' G_J^2(\boldsymbol{x},\boldsymbol{x}')\\ &= \alpha_J r_J^2 \overline{G_J^2}(\boldsymbol{x})\sigma^2_{IM}.\end{aligned} \tag{5}$$

In eq. (5), we express σ^2_{IM} by $\langle I_M\rangle$ according to eq. (2), and substitute $\langle I_M\rangle$ by $\langle V_J(\boldsymbol{x})\rangle$ according to eq. (4). We obtain a parabolic relation between the variance of the voltage and the expectation value according to

$$\sigma^2_{VJ}(\boldsymbol{x}) = v(\boldsymbol{x})\langle V_J(\boldsymbol{x})\rangle - N_v^{-1}(\boldsymbol{x})\langle V_J(\boldsymbol{x})\rangle^2, \tag{6}$$

$$v(\boldsymbol{x}) = i_{ch} r_J \frac{\overline{G_J^2}(\boldsymbol{x})}{\overline{G_J}(\boldsymbol{x})} = i_{ch}\frac{\sigma^2_{VJ}/\sigma^2_{IM}}{\langle V_J\rangle/\langle I_M\rangle}, \tag{7}$$

$$N_v(\boldsymbol{x}) = N_{ch}\alpha_J \frac{\overline{G_J}^2(\boldsymbol{x})}{\overline{G_J^2}(\boldsymbol{x})} = N_{ch}\frac{\langle V_J\rangle^2/\langle I_M\rangle^2}{\sigma^2_{VJ}/\sigma^2_{IM}}. \tag{8}$$

Equation (6) has the same structure as eq. (2) for the membrane current. It reflects the binomial statistics that results from the transformation of the membrane current to an extracellular voltage. The coefficient of the linear term represents the effective magnitude of the voltage quanta according to eq. (7); the coefficient of the quadratic term represents the effective number N_v of the voltage quanta according to eq. (8) with a relation $vN_v = \alpha_J r_J \overline{G_J} i_{ch} N_{ch}$ for the maximum voltage. The second parts of eqs. (7) and (8) are obtained when eqs. (4) and (5) are introduced. They reveal that the relation between the quanta of voltage and current can be obtained from measured averages and variances without assigning a sheet resistance r_J, a relative area α_J, a shape of the junction, and a recording position $\boldsymbol{x}$.

Experimental. – We used electrolyte-oxide-semiconductor field-effect transistors (EOSFET) with a p-channel (gate area 6 μm × 7 μm) [23]. In a final step of processing, an 11 nm film of TiO_2 was deposited on

top of the SiO_2 surface by Atomic Layer Deposition (ASM, Helsinki, Finland) [24,25]. TiO_2 was able to suppress the slow transistor response that is caused by the binding of K^+ ions to SiO_2 [14,15]. By plasma etching and wet etching with HF, TiO_2 and SiO_2 were removed on the bond pads that were then coated by sputtering with an Al/Si alloy. After tempering (4 min, 470 °C in 90% N_2, 10% O_2), the chips (8.2 mm × 8.5 mm) were wire-bonded to a ceramic package, and a Perspex chamber was attached with a silicone adhesive. The chips were cleaned with an alkaline detergent at 80 °C (5% Tickopur R36, Stamm, Berlin) using cotton swabs, rinsed with pure water, and sterilised (20 min, 70% ethanol). Fibronectin (F2006-1MG, Sigma) was adsorbed (2 h, 37 °C, 5% CO_2) from a 12 μg/ml solution in Dulbecco's Phosphate Buffered Saline (14040-091, Invitrogen).

We used the potassium channel Shaker B with a deletion Δ6-46 and a mutation T449V to suppress the N-type and the C-type inactivation [17–19]. The cDNA (gift by S. H. Heinemann) was inserted into the multiple cloning site of the pcDNA3.1/Hygro(+) vector (V870-20, Invitrogen). We cultured the HEK293-type tsA201 cells (96121229, Sigma) in Dulbecco's modified Eagle's medium (DMEM, high glucose, D6546 Sigma) with 2 mM L-Glutamine and 10% (vol/vol) heat-inactivated fetal bovine serum (FBS, 10270-106, Invitrogen) (37 °C, 5% CO_2), and transfected them (calcium phosphate method). A stable monoclonal cell line was established by selection with 0.4 mg/ml Hygromycin B (10687-010, Invitrogen), picking single clones via limiting dilution, and screening for apt whole cell currents by patch-clamp recordings. Cells of the monoclonal cell line were cultured to 70%–80% confluency, isolated with a cell dissociation solution (C5789, Sigma) and plated on a chip for several hours in DMEM without FBS and Hygromycin B. Before a measurement, the culture medium was replaced by an extracellular medium with (in mM) 135 NaCl, 5 KCl, 1.8 $CaCl_2$, 1 $MgCl_2$ and 5 HEPES (adjustments to *p*H 7.4 with NaOH, to 320 mOsmol/kg with glucose).

Patch pipettes were pulled from borosilicate glass (Science Products, Hofheim, Germany), filled with an intracellular medium with (in mM) 140 KCl, 5 HEPES, and 1 EGTA (adjustments to *p*H 7.4 with KOH, to 330 mOsmol/kg with glucose), and contacted with a chlorinated silver wire (pipette resistance 2–3 MΩ). A cell on a transistor was selected (Axioskop 2FS, Zeiss), and a whole-cell pipette contact was established. The intracellular voltage was held at −60 mV with respect to an Ag/AgCl electrode in the bath (World Precision Instruments, Berlin, Germany). An EPC10 amplifier (HEKA Elektronik, Lambrecht, Germany) recorded the pipette current $I_{\rm Pip}$. The capacitance transient cancellation was activated and the series resistance compensation was set to 80%. The chip was connected to a custom built amplifier (200 kHz bandwidth). The operating point of each transistor was set by applying +0.1 V to the source/bulk silicon and −0.5 V to drain with respect to the bath electrode with a drain current $I_{\rm FET} \approx -10\,\mu$A and a transconductance $g_{\rm m} \approx 20\,\mu$S. Changes of the drain current in an experiment were expressed in terms of a transistor voltage with $V_{\rm FET} = \delta I_{\rm FET}/g_{\rm m}$. We applied depolarizations to −20 mV, 0 mV, and +20 mV to a cell for 10 ms, each with a P/4 protocol. The stimuli were repeated 256 times within 200 s. Pipette current and transistor voltage were sampled at 400 kHz (NI USB-6259, National Instruments) and filtered at 10 kHz with a 2nd-order Butterworth filter.

From the ensemble of 256 recordings, the average and the variance of the pipette current $I_{\rm Pip}$ as well as of the transistor voltage $V_{\rm FET}$ were estimated for a time interval where the average current increased and where the effects of the stimulus and of a changing ion concentration in the junction [14] were negligible. With the P/4 prepulse recordings, the effect of the leak current and of capacitive transients were eliminated from the averages of pipette current and transistor voltage. To reduce the influence of drift and run-down, a pairwise estimator was used to estimate the ensemble variance and autocovariance [20]. Average and variance of the pipette current were grouped into suitable bins [21]. The same time intervals were used to group the average and the variance of the transistor voltage.

The averages of current and voltage as well as the variances were compared with each other. To estimate the magnitude and number of the current quanta, we fitted the current data with the estimated generalised least squares (EGLS) approach [22] implemented with SAGE [26]. We used the parabolic relation of eq. (2) with a background as $\sigma^2_{\rm Pip} = \sigma^2_{\rm IM} + \sigma^2_{\rm Pip,bg}$. In analogy we fitted the voltage data according to eq. (6) with $\sigma^2_{\rm FET} = \sigma^2_{\rm VJ} + \sigma^2_{\rm FET,bg}$ where the background includes effects of the transistor and of the junction. Extending the original EGLS approach, the data for two depolarizations were simultaneously fitted with a common number of quanta and a common background of the voltage variance.

Results. – The following set of results was obtained for the cell that is depicted in fig. 1(b). The pipette current $I_{\rm Pip}(t)$ is plotted in fig. 2(a) *vs.* time for the two intracellular voltages $V_{\rm M}^{(1)} = 20$ mV and $V_{\rm M}^{(2)} = 0$ mV. The current increased within a few milliseconds to a rather stationary level with some rundown that is due to the long duration (200 s) of the measurement and the large number of stimulations. Simultaneously, the transistor voltage $V_{\rm FET}(t)$ was recorded as shown in fig. 2(b). It increased with a similar dynamics as the membrane current. After a few milliseconds, however, the signal dropped, an effect that is due an enhanced extracellular K^+ concentration that reduces the driving force of the current (electrodiffusion) [14]. For the evaluation of the nonstationary signals, we a selected a time interval where that effect played no role (see fig. 2).

In fig. 3(a), the ensemble average $\langle V_{\rm FET}\rangle$ is plotted *vs.* the ensemble average $\langle I_{\rm Pip}\rangle$ for two intracellular

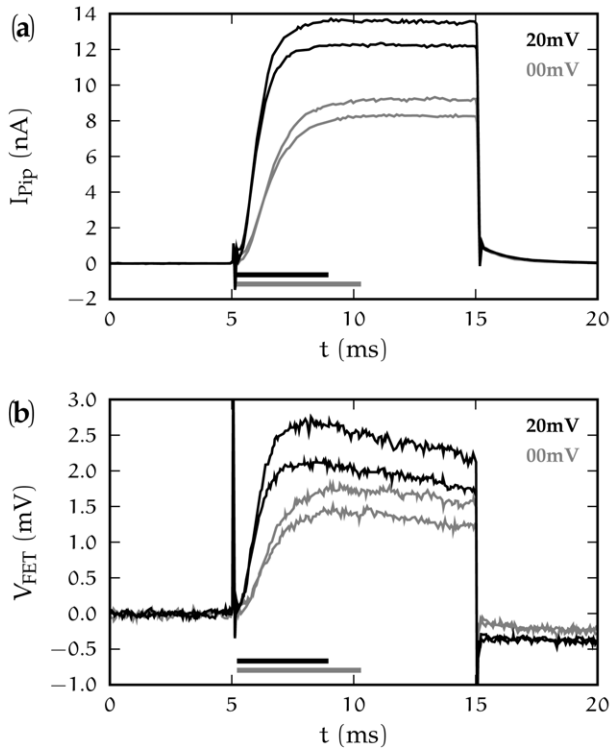

Fig. 2: Pipette current and transistor voltage. (a) Pipette current I_{Pip} *vs.* time upon application of an intracellular voltage of 20 mV (black) and 0 mV (grey) for 10 ms, starting from a holding voltage of −60 mV. The first and last traces of 256 stimulations are plotted. (b) Transistor voltage V_{FET} *vs.* time for the same experiment (with capacitive transients). For the pipette current and for the transistor voltage the evaluation of the noise is limited to the time interval marked by the bars where the current and the voltage are nonstationary and where effects of stimulation and of changing ion concentration are excluded.

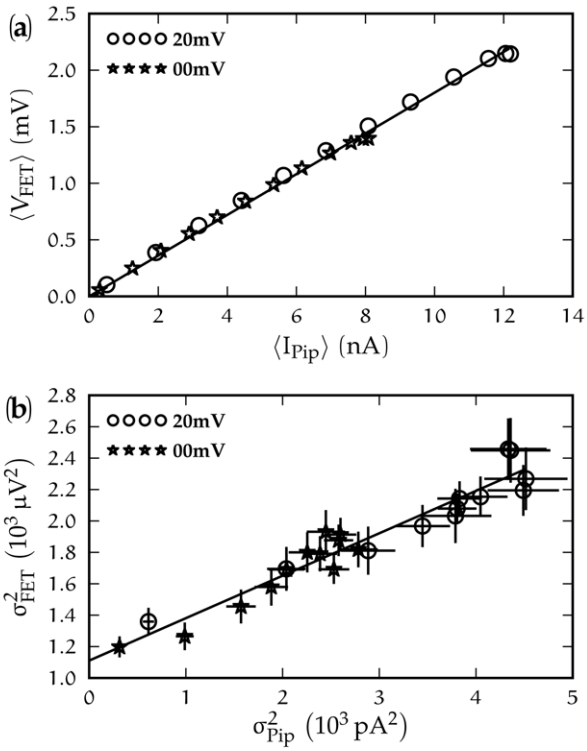

Fig. 3: Relation between transistor voltage and pipette current. (a) Ensemble average of the transistor voltage *vs.* ensemble average of the pipette current for intracellular voltages 20 mV and 0 mV. The data are fitted by a linear relation with a slope of 0.180 MΩ. (b) Ensemble variance of the transistor voltage *vs.* ensemble variance of the pipette current. The bars indicate the standard error of the bins [22]. The data are fitted by a linear relation with a slope of 0.273 MΩ^2 and a background of 1100 μV^2.

voltages after subtracting the leak currents. The data were fitted by a relation $\langle V_{\mathrm{FET}}\rangle = (0.180 \pm 0.001)\,\mathrm{M\Omega} \cdot \langle I_{\mathrm{Pip}}\rangle$. This proportionality indicates that the transistor signal reflects an extracellular voltage that is caused by the membrane current flowing through the pipette according to eq. (4) with $\langle V_{\mathrm{J}}\rangle \approx 0.18\,\mathrm{M\Omega} \cdot \langle I_{\mathrm{M}}\rangle$. In fig. 3(b), the ensemble variance σ^2_{FET} is plotted *vs.* the ensemble variance σ^2_{Pip}. The data were fitted by a relation $\sigma^2_{\mathrm{FET}} = (0.273 \pm 0.006)\,\mathrm{M\Omega}^2 \cdot \sigma^2_{\mathrm{Pip}} + \sigma^2_{\mathrm{bg}}$, taking into account the background noise of voltage and current. This fit reflects a proportionality of the variances of voltage and current according to eq. (5) with $\sigma^2_{\mathrm{VJ}} \approx 0.27\,\mathrm{M\Omega}^2 \cdot \sigma^2_{\mathrm{IM}}$. If we accept binomial statistics, the proportionalities between the averages and between the variances determine relations between the magnitudes of the quanta and between their numbers according to eqs. (7) and (8). With the fitted parameters, we obtain $v \approx 1.5\,\mathrm{M\Omega} \cdot i_{\mathrm{ch}}$ and $N_{\mathrm{v}} \approx 0.12 \cdot N_{\mathrm{ch}}$.

In a second step, we checked the binomial statistics. In fig. 4(a) the variance of the pipette current σ^2_{Pip} is plotted *vs.* the average $\langle I_{\mathrm{Pip}}\rangle$. The data for both intracellular voltages were simultaneously fitted by parabolas with two current quanta, a common channel number, and two background variances as parameters. We obtained the current quanta $i^{(1)}_{\mathrm{ch}} = (1.064 \pm 0.083)\,\mathrm{pA}$, $i^{(2)}_{\mathrm{ch}} = (0.815 \pm 0.054)\,\mathrm{pA}$, and a channel number $N_{\mathrm{ch}} = 15700 \pm 1700$. With the relation $i_{\mathrm{ch}} = \gamma_{\mathrm{ch}} \cdot (V_{\mathrm{M}} - V_0^{\mathrm{K}})$ and a reversal voltage $V_0^{\mathrm{K}} = -85\,\mathrm{mV}$, the channel conductance was $\gamma_{\mathrm{ch}} = (9.9 \pm 0.3)\,\mathrm{pS}$ in good agreement with the literature [27,28]. In fig. 5(b), the variance of the transistor voltage σ^2_{FET} is plotted *vs.* the average $\langle V_{\mathrm{FET}}\rangle$. The data for the two intracellular voltages were simultaneously fitted by parabolas with two voltage quanta, a common number of quanta and a common background variance as parameters. We obtained the voltage quanta $v^{(1)} = (1.49 \pm 0.34)\,\mu\mathrm{V}$, $v^{(2)} = (1.20 \pm 0.26)\,\mu\mathrm{V}$, and a number of quanta $N_{\mathrm{v}} = 2020 \pm 630$. The results of these parabola fits imply the relations $v^{(1)} \approx 1.40\,\mathrm{M\Omega} \cdot i^{(1)}_{\mathrm{ch}}$, $v^{(2)} \approx 1.47\,\mathrm{M\Omega} \cdot i^{(2)}_{\mathrm{ch}}$, and $N_{\mathrm{v}} \approx 0.13 \cdot N_{\mathrm{ch}}$; within the error of the measurements, they are compatible with the relations obtained from the slopes $\langle V_{\mathrm{J}}\rangle / \langle I_{\mathrm{M}}\rangle$ and $\sigma^2_{\mathrm{VJ}} / \sigma^2_{\mathrm{IM}}$.

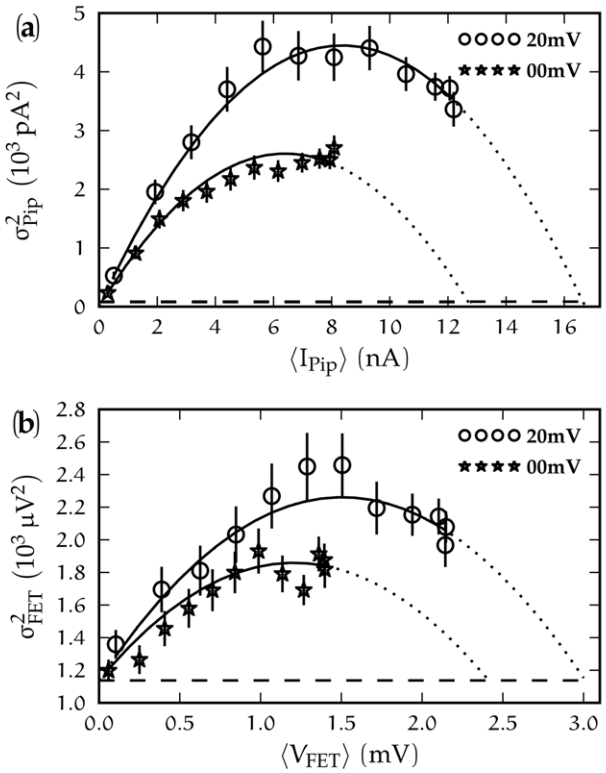

Fig. 4: Test for binomial statistics of pipette current and transistor voltage. (a) Ensemble variance of the pipette current *vs.* the ensemble average. The bars indicate the standard error of the bins [22]. The data at the intracellular voltages of 20 mV and 0 mV are fitted by two parabolas (drawn and dotted lines) with backgrounds of 85 pA^2 and 78 pA^2 (dashed line). (b) Ensemble variance of the transistor voltage *vs.* the ensemble average. The data are fitted by two parabolas with a common background of $(1140 \pm 100)\,\mu$V^2 (dashed line).

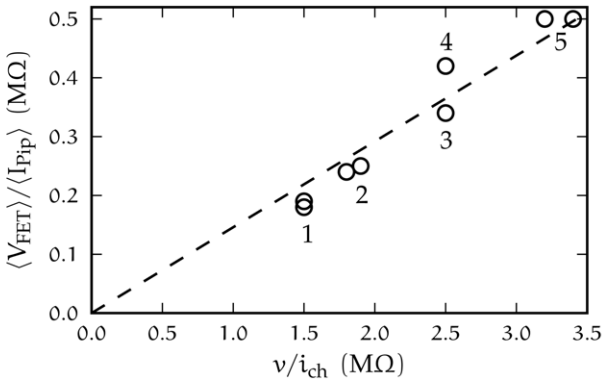

Fig. 5: Resistance parameter $\langle V_J\rangle/\langle I_M\rangle$ for the averages of voltage and current *vs.* resistance parameter v/i_{ch} for the quanta as obtained from the linear plots (see fig. 3) for eight measurements with five cells. The data are fitted by a linear relation with a slope 0.15.

With about 100 chips we found on average one healthy cell in a suitable position on a transistor. A good access by the patch pipette was achieved for 40 cells with a sufficient ion current and transistor signal. During the noise measurement or on the later inspection of the data we found, however, that only five cells were long-term stable enough for a successful evaluation of the conventional nonstationary noise of the pipette current. So we performed the complete noise analysis on those five cell-transistor assemblies. Besides the recordings as described above, we were able to conduct another run with 256 depolarisations to 40 mV on cells with exceptionally stable seals resulting in a total of eight measurements. The slopes obtained from the plots of the averages and variances (as in fig. 3) are presented in fig. 5 in terms of a resistance parameter $\langle V_J\rangle/\langle I_M\rangle$ of the averages and a resistance parameter $\sigma^2_{VJ}/\sigma^2_{IM}/(\langle V_J\rangle/\langle I_M\rangle) = v/i_{ch}$ of the quanta. Both parameters vary by a factor of two to three; they are linearly correlated with a slope of 0.15.

Discussion. – The voltage quantum of $v \approx 1\,\mu$V is determined by the channel quantum $i_{ch} \approx 1$ pA. It represents an average of the individual quanta that are created in the cell-chip junction at the position of the transistor. The magnitude v and the number N_v of the voltage quanta depend on the properties of the cell-chip junction according to eqs. (7) and (8) with a sheet resistance r_J, a relative area α_J, and a recording position $\boldsymbol{x}$ in a junction with a certain shape. As a model, we consider a circular junction of radius a_J, which is matched to the cell-chip junction as illustrated in fig. 1(b). The Green's function of the Poisson equation with Dirichlet boundary conditions is given in polar coordinates by [29]

$$G_J(a,\varphi,a',\varphi') = -\frac{1}{4\pi}\ln\left(a_J^2\frac{a^2+a'^2-2aa'\cos(\varphi-\varphi')}{a^2a'^2+a_J^4-2aa'a_J^2\cos(\varphi-\varphi')}\right). \quad (9)$$

At first, we consider a local voltage recording in the centre at $a = 0$. Analytical integration of eq. (9) yields the spatial averages $\overline{G_J} = 1/4\pi$, $\overline{G_J^2} = 1/8\pi^2$. With eqs. (7) and (8), the magnitude and number of the voltage quanta are $v = i_{ch}r_J/2\pi$ and $N_v = N_{ch}\alpha_J/2$, respectively. Using the results of fig. 3 these relations yield a sheet resistance $r_J = 9.5\,$MΩ and a relative area $\alpha_J = 0.24$. As indicated in fig. 1(b), the recording transistor was at an eccentric position $a/a_J \approx 2/3$ of the circular model. For eccentric recordings, we evaluated the spatial averages of $G_J(\boldsymbol{x})$ and $G_J^2(\boldsymbol{x})$ by analytical and numerical integration, respectivly. The radial profiles are plotted in fig. 6. At a position $a/a_J = 2/3$ we obtained $\overline{G_J^2}/\overline{G_J} = 0.75/2\pi$ and $\overline{G_J}^2/\overline{G_J^2} = 0.76/2$; and the magnitude and number of the voltage quanta are $v = 0.12 \cdot i_{ch}r_J$ and $N_v = 0.38 \cdot N_{ch}\alpha_J$. Using the results of fig. 3 these relations yield a sheet resistance $r_J = 12.6\,$MΩ and a relative area $\alpha_J = 0.31$. The relative area corresponds well to a hemispherical cell. The sheet resistance is similar to values obtained by AC stimulation [14]. With a resistivity 67 Ωcm of the bath, it corresponds to an electrolyte film of 53 nm in good agreement with optical measurements for similar conditions [14].

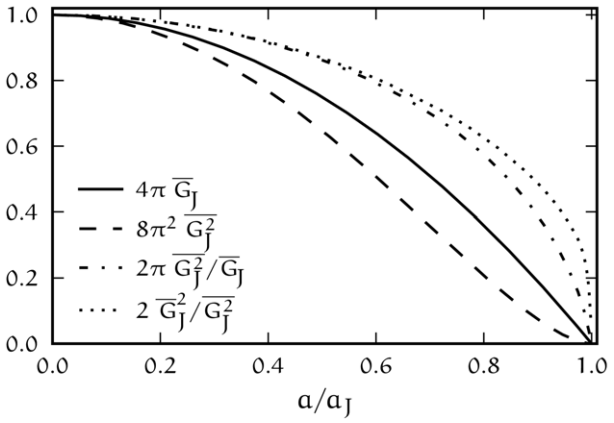

Fig. 6: Various spatial averages of the Green's function G_J for recording positions along the radius of a circular cell-solid junction. The coordinate a is normalised to the radius a_J of the junction. The profiles are normalised to the values in the centre.

A striking feature of the results in fig. 5 is the correlation of the resistance parameters $\langle V_J\rangle/\langle I_M\rangle$ and v/i_{ch}. Considering eq. (8), the proportionality indicates a relation $\alpha_J\overline{G_J}^2/\overline{G_J^2} = 0.15$. Apparently the combined effect of the relative area and of the recording position is similar in the different systems, possibly due to a biased selection of successful cell/transistor assemblies. The variability of the results must be dominated by the sheet resistance r_J that depends on the individual biological properties of the cell-solid interaction.

Conclusion. – i) Voltage fluctuations exist in the area of cell adhesion, which can be attributed to fluctuations of the membrane current. ii) The voltage fluctuations can be interpreted in terms of voltage quanta that obey binomial statistics. Their magnitude is determined by the current quanta of the ion channels, by the position of recording in the core-coat conductor, and the shape of the cell-solid junction. iii) By evaluating the fluctuating voltage, the two crucial parameters of a cell-chip junction, the sheet resistance r_J and the relative area α_J, can be determined in a single type of experiment. iv) The successful interpretation of the fluctuating transistor voltage in terms of the fluctuating membrane current confirms that the transistor signal reflects a voltage caused by ion current, not a change of the surface potential.

* * *

We thank E. Tois (ASM, Helsinki) for the atomic layer deposition of TiO_2, A. Lambacher and F. Felderer for support with chip processing, S. H. Heinemann (University Jena) for the cDNA of the Shaker channel, and K. Scheidt, M. Morawetz, and S. Stumhofer for expert help with molecular biology, R. Zeitler for useful discussions and again A. Lambacher for critical reading of the manuscript.

REFERENCES

[1] Prost J. and Bruinsma R., *Europhys. Lett.*, **33** (1996) 321.
[2] Ries J., Petrov E. P. and Schwille P., *Biophys. J.*, **95** (2008) 390.
[3] Hilt M. and Zimmermann W., *Phys. Rev. E*, **75** (2007) 016202.
[4] Medalia O. and Geiger B., *Curr. Opin. Cell Biol.*, **22** (2010) 659.
[5] Giaever I. and Keese C. R., *Proc. Natl. Acad. Sci. U.S.A.*, **88** (1991) 7896.
[6] Domanska M. K., Kiessling V. and Tamm L. K., *Biophys. J.*, **99** (2010) 2936.
[7] Fromherz P., *Solid-State Electron.*, **52** (2008) 1364.
[8] Katz B. and Miledi R., *J. Physiol. (London)*, **224** (1972) 665.
[9] Neher E. and Sakmann B., *Nature*, **260** (1976) 799.
[10] Sigworth F. J., *Nature*, **270** (1977) 265.
[11] Weis R. and Fromherz P., *Phys. Rev. E*, **55** (1997) 877.
[12] Schätzthauer R. and Fromherz P., *Eur. J. Neurosci.*, **10** (1998) 1956.
[13] Straub B., Meyer E. and Fromherz P., *Nat. Biotechnol.*, **19** (2001) 121.
[14] Brittinger M. and Fromherz P., *Appl. Phys. A*, **81** (2005) 439.
[15] Peitz I. and Fromherz P., *Eur. Phys. E*, **30** (2009) 223.
[16] Voelker M. and Fromherz P., *Phys. Rev. Lett.*, **96** (2006) 228102.
[17] Hoshi T., Zagotta W. and Aldrich R., *Science*, **250** (1990) 533.
[18] López-Barneo J., Hoshi T., Heinemann S. H. and Aldrich R. W., *Recept. Channels*, **1** (1993) 61.
[19] Starkus J. G., Varga Z., Schönherr R. and Heinemann S. H., *Eur. J. Physiol.*, **447** (2003) 44.
[20] Sigworth F. J., *Biophys. J.*, **35** (1981) 289.
[21] Heinemann S. H. and Conti F., *Methods Enzymol.*, **207** (1992) 131.
[22] Steffan R. and Heinemann S. H., *J. Neurosci. Methods*, **78** (1997) 51.
[23] Voelker M. and Fromherz P., *Small*, **1** (2005) 206.
[24] Hutzler M. and Fromherz P., *Eur. J. Neurosci.*, **19** (2004) 2231.
[25] Wallrapp F. and Fromherz P., *J. Appl. Phys.*, **99** (2006) 114103.
[26] Stein W. *et al.*, *Sage Mathematics Software (Version 4.1)*, The Sage Development Team, `http://www.sagemath.org` (2009).
[27] Iverson L. E., Tanouye M. A., Lester H. A., Davidson N. and Rudy B., *Proc. Natl. Acad. Sci. U.S.A.*, **85** (1988) 5723.
[28] Heginbotham L. and MacKinnon R., *Biophys. J.*, **65** (1993) 2089.
[29] Haberman R., *Applied Partial Differential Equations*, 4th edition (Pearson Education, Upper Saddle River, NJ) 2004, p. 432.